JACS
JOURNAL OF THE AMERICAN CHEMICAL SOCIETY

Article

A responsive MRI contrast agent for detection of excess copper(II) in the liver in vivo

Namini N. Paranawithana, Andre F Martins, Veronica Clavijo Jordan, Piyu Zhao, Sara Chirayil, Gabriele Meloni, and A. Dean Sherry

J. Am. Chem. Soc., **Just Accepted Manuscript** • DOI: 10.1021/jacs.8b13493 • Publication Date (Web): 20 Jun 2019

Just Accepted

is published by the American Chemical Society. 1155 Sixteenth Street N.W., Washington, DC 20036

A responsive MRI contrast agent for detection of excess copper (II) in the liver *in vivo*

Namini N. Paranawithana,[1] Andre F. Martins,[1] Veronica Clavijo Jordan,[2] Piyu Zhao,[1] Sara Chirayil,[2] Gabriele Meloni[1] and A. Dean Sherry[1,2]*.

[1]Department of Chemistry and Biochemistry, University of Texas at Dallas, Richardson, Texas, USA.

[2]Advanced Imaging Research Center, University of Texas Southwestern Medical Center, Dallas, Texas, USA.

KEYWORDS: Copper-responsive, Magnetic Resonance Imaging, Contrast agents, Human serum albumin, Wilson disease.

ABSTRACT: The design, synthesis, and properties of a new gadolinium-based copper-responsive MRI contrast agent is presented. The sensor (GdL_1) has high selectivity for copper ions and exhibits a 43% increase in r_1 relaxivity (20 MHz) upon binding to 1 equivalent of Cu^{2+} in aqueous buffer. Interestingly, in the presence of physiological levels of human serum albumin (HSA), the r_1 relaxivity is amplified further up to 270%. Additional spectroscopic and XAS studies show that Cu^{2+} is coordinated by two carboxylic acid groups and the single amine group on an appended side-chain of GdL_1 and forms a ternary complex with HSA (GdL_1-Cu^{2+}-HSA). T_1-weighted *in vivo* imaging demonstrates that GdL_1 can detect basal, endogenous labile copper(II) ions in living mice. This offers a unique opportunity to explore the role of copper ions in the development and progression of neurological diseases such as Wilson's disease.

1. INTRODUCTION.

Copper is the third most abundant transition metal in the body and a required dietary nutrient. The average healthy human has a total of ~110mg of copper in tissue.[1-4] Copper is typically bound to specific proteins and enzymes where it plays fundamental catalytic and structural roles.[5-7] Copper has also been associated with signaling events in the brain.[8-10] In biological environment, copper is present in two oxidation states, the cuprous (Cu^{+}) and cupric (Cu^{2+}) ions.[11] Typically, total extracellular Cu^{2+} can vary widely from nM to µM while intracellular Cu^{+} can vary from µM to mM.[12-14] Due to its redox properties, copper homeostasis is tightly regulated in cells and disruption of this is associated with a number of neurodegenerative diseases including Alzheimer's, Parkinson's, prion diseases, familial amyotrophic lateral sclerosis, Menkes and Wilson's diseases.[15-18] For instance, genetic mutations of copper-transporting proteins ATP7A and ATP7B results in afflictions of systemic brain copper deficiency in Menkes disease and hyperaccumulation of hepatic copper ions in Wilson's disease, respectively.[19-22] Accumulation of copper in the liver of Wilson's disease patients ranges from a few micromolar to several millimolar.[23] Although copper ion homeostasis and the impact of abnormal copper levels on physiology have been widely studied, details about the functional role of copper ions in various tissues *in vivo* remain insufficiently understood due to lack of real-time copper imaging techniques in live animals.[24,25]

Magnetic resonance imaging (MRI) is a powerful medical diagnostic technique that allows noninvasive, three-dimensional visualization of tissue with high spatial and temporal resolution. MRI is largely based on detection of water and fat protons so that image contrast among tissues reflects differences in proton content, cell density, and water perfusion and diffusion. Image contrast can be altered by the use of paramagnetic inorganic complexes that shorten the $T_{1,2}$ relaxation times of water molecules in various compartments. These agents are commonly known as contrast agents (CAs). Among all paramagnetic complexes designed for use as CAs, the

Gd^{3+}-based agents have proven to be the safest and most versatile agents for clinical use over the past ~30 years. The efficiency of an agent per unit concentration is commonly reported as r_1 (T_1) or r_2 (T_2) relaxivity.[26-28] Notably, the design of contrast agents that alter the T_1 of water protons in response to a given analyte is of major importance. Many responsive probes have been reported including sensors for metal ions,[9] enzyme activity,[29] pH,[30] pO_2,[31] and temperature.[32] One of the first reports of a copper-activated MR sensor was based on a GdDO3A (1,4,7,10-tetraazacyclododecane-1,4,7,-triacetic acid) derivative having a iminodiacetate pendant arm for Cu^{2+} recognition. This derivative displayed a 41% increase in r_1 relaxivity upon binding Cu^{2+}.[33] A later paper reported a GdDO3A derivative having a quinolone-based pendant arm[34] and it displayed a 71% increase in r_1 upon addition of Cu^{2+}. Neither of these agents were examined *in vivo*. Derivatives have also been designed to show greater selectivity for Cu^{+} over Cu^{2+}.[35] In addition to MRI agents, other imaging approaches for imaging copper have included positron emission tomography (PET), optical imaging and bimodal imaging techniques.[36,37] The positron emitter, ^{64}Cu, was successfully used to image greater uptake and accumulation of copper in livers of Wilson's disease mouse model.[24] Similarly, a near-infrared fluorescent sensor for detection of Cu^{+} ions has been shown to be capable of monitoring fluctuations in exchangeable copper stores in

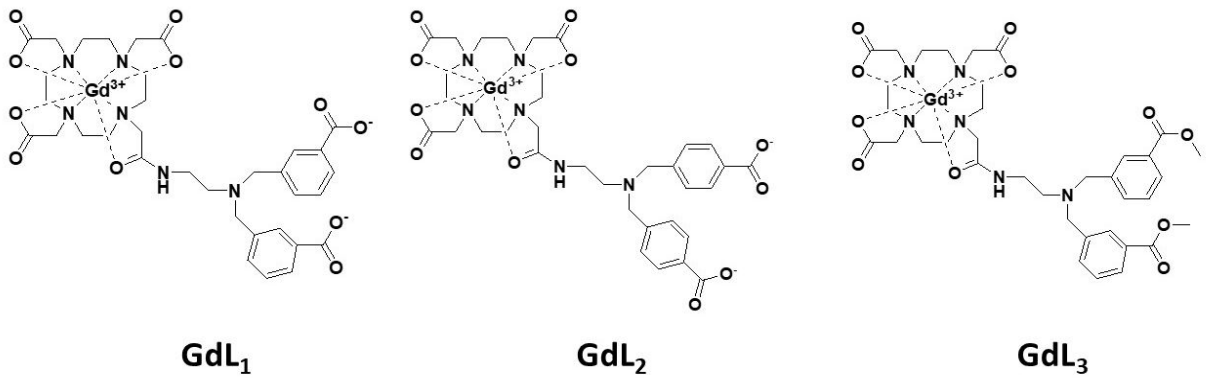

Figure 1. Gadolinium-DO3A based copper responsive (GdL) agents

living cells and mice under basal conditions, as well as in situations of copper overload or deficiency.[38]

Our group recently reported several MR zinc-sensors capable of detecting the release of intracellular stores of zinc into extracellular space in prostate[39] and pancreas of live mice.[40] Divalent zinc ions released by cells in these organs are immediately chelated by a zinc-responsive MR agent, and the resulting binary complex then forms a ternary complex with serum albumin which results in reduced molecular motion and an increase of r_1.[41,42] Copper is also known to bind to albumin and other less abundant proteins in plasma.[43-47] Hence, we hypothesized that the key to an effective copper detection *in vivo* by MRI might be to design a Cu-responsive agent that also forms a ternary complex between Cu^{2+} ions, the sensor, and albumin, similar to the Zn-sensor designs.

Herein, we report the synthesis of a novel copper-responsive MRI contrast agent having a bis(benzoic acid)methylamine recognition motif (GdL_1) and the physicochemical properties of the resulting GdL_1-Cu^{2+} complex and the ternary complex formed with HSA. X-ray absorption spectroscopy (XAS) of GdL_1 and some structural analogs were used to interrogate the Cu^{2+} binding site in this system. Finally, GdL_1 was injected into mice to detect extracellular Cu^{2+} in the liver by MRI. A comparison of GdL_1 (high Cu^{2+} affinity) with GdL_2 and GdL_3 (lower Cu^{2+} affinity) (Figure 1) indicated that only GdL_1 detects extracellular copper in mouse liver.

2. RESULTS and DISCUSSION

Design and synthesis. The structure of the Cu^{2+}-responsive agent reported here consists of a GdDO3A moiety with a bis(benzoic acid)methylamine side-chain as a potential chelator for Cu^{2+}. This design was motivated by our previous MR-responsive Zn^{2+} sensor scaffold where the ion of interest initiates formation of a ternary complex between the agent and serum albumin.[41,42] Although Cu^{2+} has a preference for nitrogen donor atoms, the coordination rigidity provided by the bis(benzoic acid)methylamine could potentially favor coordination by geometrical stabilization of tetragonal or square pyramidal structures typical of Cu^{2+}.[48,49] This structural feature precludes the possibility of binding with the more abundant biological ions like Ca^{2+} and Mg^{2+}. To evaluate the impact of repositioning of the carboxylate groups on the aromatic side-chain and lowering the charge on the carboxylate groups, GdL_2 and GdL_3 were also studied for comparison. The synthetic details of all three contrast agents are described in supplementary materials.

Water proton relaxivity measure,ments in the presence of various metal ions. The longitudinal relaxivity (r_1) of GdL_1 (4.7 ± 0.1 $mM^{-1}s^{-1}$ at 20 MHz) was unchanged upon addition of Ca^{2+}, Mg^{2+}, Cu^{+} or Fe^{3+} ions (Figure 2 and Figure S4). However, addition of Zn^{2+} increased r_1 to 5.3 $mM^{-1}s^{-1}$ (a 12% increase) while addition of Cu^{2+} increased the r_1 to 6.7 $mM^{-1}s^{-1}$ (a 47% increase). The background relaxivity due to the weak paramagnetism of Cu^{2+} and Fe^{3+} was subtracted from the r_1 values shown in Figure 2 and reported in Table 1.[50] This suggests that GdL_1 has some selectivity for Cu^{2+} over Zn^{2+} in agreement with the Irving-William series and Pearson's Hard-Soft Acid Base (HSAB) theories.[51] Even though the origin of this r_1 enhancement is unclear from these data alone, one possibility is that the linker side-arm with the anionic carboxyl groups on the bis-benzoic acid motif may form a hydrogen bond with the single exchanging inner-sphere water molecule on the Gd^{3+} ion and this interaction is reduced when Cu^{2+} or Zn^{2+} binds to GdL_1. This could in principle alter the water exchange rate in this system and result in a small change in r_1. A second contributing factor might be that GdL_1 experiences relatively slower molecular rotation (τ_R) upon binding to Cu^{2+} and this could result in a slight increase in r_1 relaxivity. These two possibilities were examined in more detail below.

The binding stoichiometry between GdL_1 and Cu^{2+} was determined to be 1:1 as reported by the method of continuous variations (see Job plot, Figure S9) and by an inflection point[52] in the relaxivity data (Figure 3). This stoichiometry was assumed in all calculations of dissociation constants (K_d). The increases in r_1 of GdL_2 and GdL_3 were considerably lower upon addition of Cu^{2+} (Figure 3), suggesting that either these two complexes have a weaker affinity for Cu^{2+} or the resulting GdL_x-Cu^{2+} complexes have quite different water exchange properties.

Binding experiments in the absence of HSA (GdL_x-Cu^{2+}). The equilibrium dissociation constants (K_d) between the three GdL_x complexes and Cu^{2+} were determined by fluorescence spectroscopy by performing titrations in which Cu^{2+} was added to a buffered solution containing GdL_x. Addition of Cu^{2+} results in quenching of the intrinsic fluorescence of the benzoic acid moieties of GdL_x (Figure S11).[53,54] The resulting binding curves were fit to a 1:1 binding model to give the K_d values reported in Table 1. These data indicate that GdL_1 has the highest affinity for Cu^{2+} (84 ± 10 μM), followed by GdL_3 (352 ± 9 μM) and GdL_2 (895 ± 32 μM). This suggests that the position of the carboxyl groups (meta *versus* para) and charge of

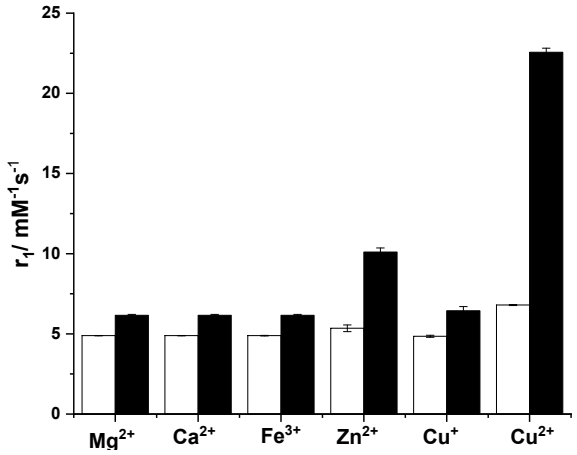

Figure 2. The 20 MHz relaxivity (r_1) of GdL_1 in the presence of various M^{n+} ± HSA. The white bars reflect r_1 after addition of 0.5 mM Mg^{2+}, Ca^{2+}, Fe^{3+}, Zn^{2+}, Cu^{+} or Cu^{2+} to 0.5mM solutions of GdL_1. The black bars reflect r_1 after subsequent addition of 0.6mM HSA to the GdL_1-M^{n+} solutions. The data were collected in 0.1M MOPS buffer (pH 7.4) at 37°C.

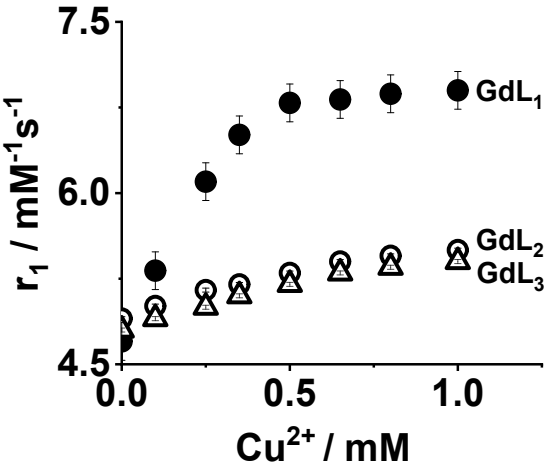

Figure 3. The 20 MHz r_1 relaxivity of $GdL_{1\text{-}3}$ as a function of added Cu^{2+}. The concentration of $GdL_{1\text{-}3}$ was 0.5 mM in 0.1M MOPS buffer (pH 7.4). The data were collected at 37°C.

the complexes are both important for Cu^{2+} binding.

Water proton relaxivity measurements in the presence of various metal ions and HSA. HSA, the most abundant protein in serum (~600 μM), plays a key role in the transport of metal ions, fatty acids, and other hydrophobic molecules including many drugs. HSA has two Cu^{2+} binding sites, the N-terminal site (NTS) and multi-metal binding site (MBS).[55,56] It was reported that Cu^{2+} has a significantly higher affinity for the NTS site (~1 pM)[57] than the MBS site (~10 nM)[58]. Thus, the NTS site is considered to be the only site in HSA to be occupied by Cu^{2+} since the concentration of HSA is much higher than the biological concentration of free Cu^{2+} ions.[55-59] We recently demonstrated that analogous Gd-based MR contrast agents responded to an increase in free Zn^{2+} ions from pancreatic β-cells[40] and epithelial prostate cells stimulated by an increase in plasma glucose.[39] This functional response was shown to reflect formation of a ternary GdL_x-Zn-albumin complex at the MBS site A.[60] This previous data suggested that perhaps Cu^{2+} could also be detected *in vivo* in those situations where excess free Cu^{2+} ions in extracellular spaces might be available for binding to a contrast agent. This motivated further relaxometric studies to determine the magnetic contributions of all the GdL_x with Cu^{2+} in the presence of physiological levels of HSA. As summarized in Table 1, the r_1 values for all three complexes increase slightly in the presence of HSA alone (likely reflecting a slight increase in viscosity) but increase substantially after the addition of Cu^{2+} ions. This suggests that the GdL_x complexes experience slower molecular rotation by the formation of a GdL_x-Cu-HSA ternary complex. This is particularly true for GdL1 where r_1 increases from 6.1 ± 0.1 to 22.6 ± 0.2 $mM^{-1}s^{-1}$ (a 270% increase). As shown in Figure 2 (and Figure S5), addition of Mg^{2+}, Ca^{2+}, Fe^{3+} do not result in an increase in r_1 in the presence of HSA while Zn^{2+} ions do to a lesser extent, about 2-fold lower than the increase in r_1 induced by Cu^{2+}.

Binding experiments in the presence of HSA. Additional proton relaxation enhancement (PRE) titrations were carried out to examine the binding interactions and to quantitatively evaluate the binding constants for each GdL_x complex with HSA in the presence of 1 molar equivalent of Cu^{2+}. A fitting of these data (Figure S13 and Table S2) to a 1:1 binding model gave the K_d values reported in Table 1. GdL_1 showed the highest binding affinity to HSA-Cu^{2+} (K_d = 45 ± 3.1 μM) while the binding affinities of GdL_2 and GdL_3 were surprisingly weaker only by ~30%. This demonstrates a significance differences in binding affinity between the different GdL_x and Cu^{2+} are leveled upon formation of the ternary GdL_x-Cu^{2+}-HSA complexes. These data alone suggest that HSA plays a significant role in stabilizing the binding interactions between GdL_x and Cu^{2+} ions. To confirm the formation of the LnL_x-Cu^{2+}-HSA ternary complex, a sample of LaL_1 (a diamagnetic analog), Cu^{2+} and HSA (from an EPR experiment, see below) were passed through a size exclusion chromatography column, and the eluent peaks were separately analyzed for Cu and La by ICP-MS. Those results (Figure S9 and Table S1) showed that ~63% of the total La eluted from the column in the form of a ternary LaL_1-Cu^{2+}-HSA complex, confirming the formation of a stable Cu mediated ternary complex.

Kinetic inertness. The kinetic stability of a GdL_x complex is also an important factor to consider when developing MRI probes. Previous studies reported that Cu^{2+} could displace Gd^{3+} from a complex by transmetallation.[61,62] This possibility was examined by challenging GdL_1 with 3-molar equivalents of Cu^{2+} in 0.03 M phosphate buffer (pH =7.2). Under these conditions, if transmetallation occurred, any unchelated Gd^{3+} would then precipitate from the solution as an insoluble phosphate, a process that can be monitored by relaxometry. R_{1obs} values measured over the time (Figure S15) show that complexes are kinetically inert, even in the presence of 3-fold excess Cu^{2+}. In addition, LC-MS data showed that in the presence of a 1-molar equivalent of Cu^{2+} no metal transmetallation was observed at room temperature after 7 days in MOPS buffer.

Table 1. 20 MHz relaxivity values for GdL_{1-3} ± Cu^{2+} and ± HSA and K_d values for binding of GdL_{1-3}-Cu^{2+} with HSA. All experiments were performed in 0.1M MOPS buffer (pH 7.4) at 37°C.

	In the absence of 0.6 mM HSA				In the presence of 0.6mM HSA			
GdLx	r_1 ($mM^{-1}s^{-1}$)		% increase in r1	K_d (GdL-Cu^{2+}) (μM)[a]	r_1 ($mM^{-1}s^{-1}$)		% increase in r_1	K_d (GdL-Cu^{2+}-HSA) (μM)[b]
	No Cu^{2+}	**1 eq. Cu^{2+}***			**No Cu^{2+}**	**1 eq. of Cu^{2+}**		
GdL_1	4.7±0.1	6.7±0.1	43%	84 ± 10	6.1±0.1 5.7±0.1[c]	22.6±0.2 15.4±0.2[c]	270%	45 ± 3.1
GdL_2	4.9±0.2	5.5± 0.1	12%	895 ± 32	6.5±0.2	14.5± 0.1	123%	59 ± 5
GdL_3	4.8±0.1	5.4±0.2	12%	352 ± 9	6.3±0.2	12.0±0.2	90%	60 ± 10

[a] $K_{d(GdL\text{-}Cu2+)}$ was determined by fluorescence titrations.
[b] $K_{d(GdL\text{-}Cu2+\text{-}HSA)}$ was determined by proton relaxation enhancement titrations.
[C] Values measured in the presence of 0.6 mM mouse albumin.

Experiments to identify the Cu^{2+} donor atoms in GdL_1. The X-band EPR spectrum of LaL_1-Cu^{2+} exhibited an unusual axial spectrum (devoid of well-defined hyperfine features and a $g_\perp \cong 1.99$) both in the absence and presence of HSA (Figure S18). The $g_\perp$ values shown by these spectra significantly deviated from the typical values of an axial EPR spectrum for Type-2 Cu^{2+} complex.[535] This suggests that the Cu^{2+} center in both complexes are electron poor, likely due to the strong electron withdrawing effect of the lanthanum ion in the complex. In comparison, the X-band EPR spectrum of HSA-Cu^{2+} exhibited a typical Type-2 square pyramidal geometry very similar to previously reported EPR spectra in the literature.[63] However, the broadened hyperfine features of the Cu^{2+} EPR spectra after addition of LaL_1 precluded a detailed structural analysis of the copper center.

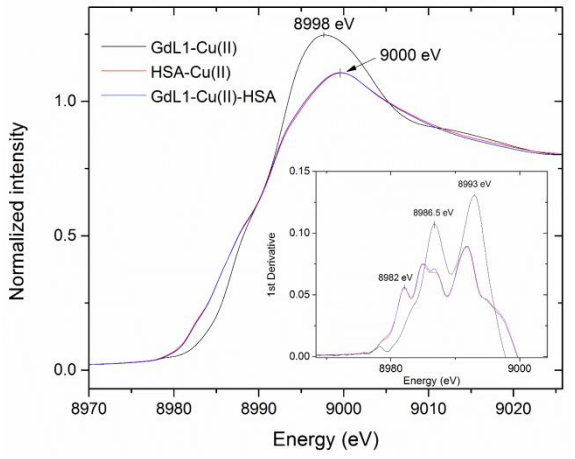

Figure 4. XANES spectra for GdL_1 in the presence of Cu^{2+} and HSA.

XAS studies. Copper K-edge X-ray absorption spectroscopy (XAS) studies were also performed to identify the Cu^{2+} donor atoms in GdL_1-Cu^{2+} and GdL_1-Cu^{2+}-HSA. The XANES spectrum of GdL_1-Cu^{2+} (Figure 4) is characterized by an intense absorption feature at 8987–8988eV with a broad low energy tail in the region below 8985eV (normalized absorption of approx. 0.5 at 8988 eV) arising from a 1s → 4p transition characteristic of Cu^{2+} complexes. The presence of the first major inflection point at 8986eV and the absence of lower energy features (normalized absorption 0.15 at 8984 eV and first inflection point 8984 eV) is typical of classic tetragonal Cu^{2+} complexes with nitrogen and oxygen ligands. The complex also presents a weak 8979eV peak (more visible in the first derivative spectra) corresponding to the 1s → 3d transition possibly reflecting a less centrosymmetric nature of the center and thus a significant degree of distortion from planarity.[64] The XANES spectrum of GdL_1-Cu^{2+}-HSA is nearly identical to the spectrum of Cu^{2+}-HSA, suggesting a very similar coordination environment in the two complexes. The spectra are characterized by an intense absorption feature at 8987–8988eV arising from a 1s → 4p transition. Additional features for the Cu^{2+} site include a lower-energy feature with normalized absorption of approximately 0.25 at 8984 eV, and the first inflection point determined in the first derivative spectrum at 8982 eV, about ~1 eV higher than the one observed in Cu^{+} complexes. Possible photoreduction of Cu^{2+} was prevented experimentally by collecting the spectra at different locations in the frozen sample in each scan. Also, the XANES spectra were quite similar to the one observed for the Cu^{2+}-DAHK peptide complex representing the N-terminal Cu^{2+} binding site in HSA, thus supporting the same coordination environment in the full-length protein.[55]

Additional information of coordination environment and ligand metal distances were obtained by copper K-edge extended X-ray absorption fine structure (EXAFS). The experimental copper EXAFS spectra are presented in Figure S19 together with best fits, and the corresponding EXAFS Fourier transforms. The spectrum of GdL_1-Cu^{2+} could be fitted with 2 ligand shells indicative of a Cu complex coordinated by 3 N/O ligands at 1.99 Å and a N/O ligand at 2.51 Å (Table 2). The XANES and EXAFS results are consistent with the formation of a distorted tetragonal complex in which 3 donor atoms from the two carboxylates and the tertiary amine of the bis(benzoic

acid)methylamine moiety with possible additional coordination by a solvent water molecule to the Cu^{2+} ion.

chelating sites in bis(benzoic acid)methylamine moiety of GdL_1. It should be noted that the bond distances for the distorted

Table 2 . Structural and coordination parameters obtained from fitting Cu K-edge EXAFS.
(N- Coordination Number, R -interatomic distance, σ^2- Debye-walker factor)

Complex	N	bond	R (Å)	σ^2(Å^2)	F-factor
GdL_1-Cu(II)	3	Cu-N/O	1.994(3)	0.0008	0.488
	1	Cu-N/O	2.51(1)	0.0001	
Cu(II)-HSA	3	Cu-N/O	1.991(2)	0.0016	0.398
	1	Cu-N/O	2.278(7)	0.0013	
	1	Cu-N/O	2.515(7)	0.0008	
GdL_1-Cu(II)-HSA	3	Cu-N/O	1.954(6)	0.0054	0.576
	1	Cu-N/O	2.33(1)	0.0037	
	1	Cu-N/O	2.86(1)	0.0001	
GdL_1-Cu(II)-HSA	4	Cu-N/O	1.965(6)	0.0054	0.587
	1	Cu-N/O	2.31(2)	0.0037	
	1	Cu-N/O	2.87(1)	0.0001	

Coordination numbers are indicated by *N*, interatomic distances *R* are given in Å (the values in parentheses are the estimated standard deviations), Debye–Waller factors σ^2 (the mean-square deviations in interatomic distance) in Å^2, and the fit-error function *F* is defined by $F = [\sum k^6(\chi(k)_{calcd} - \chi(k)_{exp})^2 / \sum k^6(\chi(k)_{exp})^2]^{1/2}$ where $\chi(k)$ are the EXAFS oscillations and *k* is the photoelectron wavenumber.

In the HSA-Cu^{2+} complex, the EXAFS data were best fit with 3 coordinating shells around Cu^{2+} with 3 Cu-O/N bonds at 1.99 Å and an additional (likely equatorial) N/O bond at 2.28 Å. In addition, a third shell corresponding to a N/O ligand at 2.51 Å was obtained in the fit suggesting the presence of an axial ligand. This analysis was in agreement with a previously reported square pyramidal Cu^{2+}-HSA coordination at the N-terminal site (also known as ATCUN) with high-affinity for Cu^{2+}.[53] Copper is coordinated to four nitrogen donors in the NTS site consisting of Asp, Ala, His amide nitrogen atoms and the His side chain in an equatorial position and a water molecule or N-terminal amine nitrogen in the axial position.[55,59] For the GdL_1-Cu^{2+}-HSA ternary complex, the EXAFS data could be best fitted with 3 or 4 N/O ligands (resulting in similar F-values) at 1.96 Å and 2 additional N/O ligands at 2.33 Å and 2.89 Å. The analysis predicts the presence of a distorted square pyramidal/ octahedral coordination around the Cu^{2+} in the ternary complex with 4 equatorial ligands with short bond distances and 1 or 2 axial ligands with longer bond distance (Table 2). This coordination anticipates the replacement of a loosely bound axial ligand in the Cu^{2+}-HSA complex by the square pyramidal Cu^{2+}-HSA complex are distinctly different from the bond distances of the distorted square pyramidal ternary complex. Despite being difficult to unambiguously distinguish the coordination 1 or 2 axial ligands by XAS, the EXAFS analysis confirms small differences in the coordination shells between GdL_1-Cu^{2+}-HSA and HSA- Cu^{2+}. This distorted octahedral or square pyramidal coordination of Cu^{2+} in the ternary complex compared to the distorted square pyramidal coordination of Cu^{2+}-HSA supports the formation of a copper-mediated complex between HSA and GdL_1.

Molecular Modelling. Molecular models of the Cu centers in GdL_1, HSA, and the ternary complex were generated based upon the coordination geometry and bond lengths for N and O atoms obtained from the EXAFS experimental data (Table 2) using standard MM+ methods. The energy-minimized models are presented in Figure 5. The model of GdL_1-Cu^{2+} reflects a distorted tetragonal geometry around the Cu center as predicted by XAS. The geometry of the NTS Cu^{2+} site in HSA reflects a square pyramidal geometry similar to the previously reported crystal structures,[53] while Cu center in the ternary complex is a distorted octahedral geometry. These models support the EPR

and XAS data by predicting only small differences in coordination geometry of GdL_1-Cu^{2+}-HSA compared to HSA-Cu^{2+}.

maximum intensity after ~6 minutes post-injection, reflective of relatively fast excretion of GdL_1 characteristic of most low molecular weight Gd-based extracellular agents. In a separate

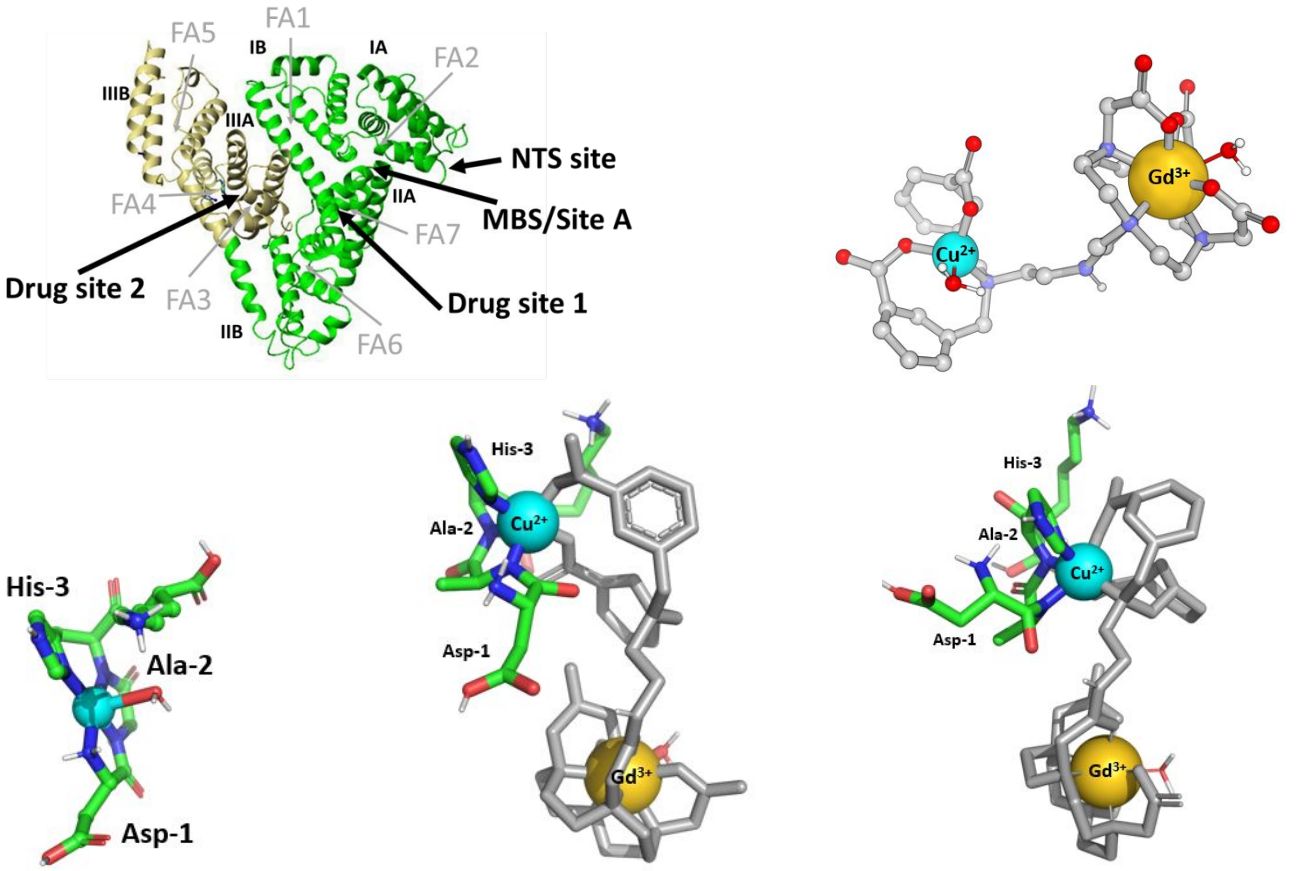

Figure 5. MM+ minimized structures of (A) Domain structure of albumin (PDB ID code 1AO6): domain I and II are colored green (residues 1–373), domain III in yellow (residues 380–571), long chain fatty acid sites (FA), Sudlow's drug binding sites, Cu^{2+} binding NTS site and zinc binding site A (MBS/Site A) are also shown. (B)GdL_1-Cu^{2+} complex (C) HSA-Cu^{2+} complex (CCDC-809109)[52] (D) HSA-Cu^{2+}- GdL_1 distorted square pyramidal complex (E) HSA-Cu^{2+}- GdL_1 distorted octahedral complex consistent with all NMR, XAS and EXAFS data. Hydrogen atoms and other sites of HSA have been removed to simplify visualization. Only residues at NTS site in HSA are included. These figures were generated using Hyperchem™7.5.

In vivo imaging of free copper pools in living mice. Most dietary absorbed copper is transported to the liver via enterohepatic circulation where serum albumin acts as transporter protein to maintain total exchangeable forms of copper in the μM range.[10,65-70] Hence, the liver plays a key role in copper homeostasis by facilitating copper storage and incorporating copper into ceruloplasmin and other copper binding proteins. Either elevated or reduced copper in the liver has been associated with neurological disorders and acute liver diseases. Therefore, a non-invasive method to image those abnormalities in copper levels *in vivo* is of broad interest.

To examine whether GdL_1 can detect and respond to changes in extracellular copper *in vivo*, T_1-weighted MR images of C57BL/6 mice were collected at 4.7T (Figure 6). This imaging field was chosen from the equipment available to us because the r_1 differences between GdL_1 *versus* GdL_1-Cu-HSA, although smaller at 4.7T *versus* 0.47T (20 MHz), remain significantly different. After i.v. injection of a bolus of 0.1 mmol/kg GdL_1, the average gain in signal intensity throughout the liver of a healthy mouse was ~25% when compared to the pre-contrast images. This enhancement returned to baseline after reaching group, mice were pretreated with the copper chelator, ATN-224 (5 mg/kg), two hours prior to injection of GdL_1.[38,70] In those animals, the average MR liver enhancement after injection of 0.1mmol/kg GdL_1 was lower, ~11% (p-value = 8.6 X 10^{-3}). This suggests that pre-treatment with the copper chelator removed some of the excess Cu^{2+} prior to injection of GdL_1. The tissue distribution of Cu and Gd in the same mice used in the imaging experiments were determined by ICP-MS analysis (Figure 6C). These results confirmed that the higher MR signal intensities directly correlated with higher copper levels in the liver of healthy mice while the Gd content was identical in both ATN-224 treated and non-treated animals.

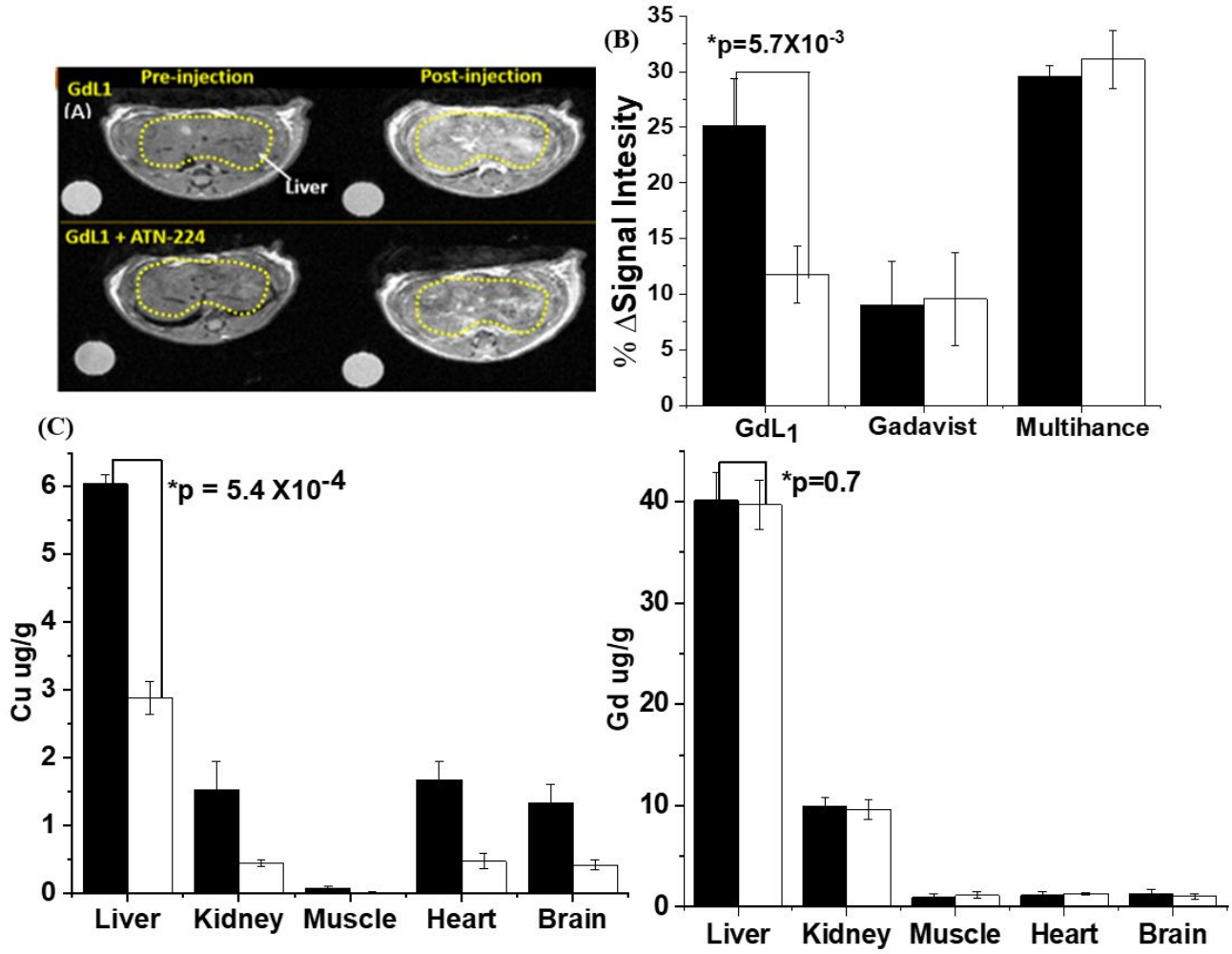

Figure 6. (A) *In vivo* MRI images of wild type mouse (n=3) pre- and post-injection of GdL_1 (0.1mmol/kg) without (top) or with (bottom) pretreatment with ATN-224 (5mg/kg in 50ul). All images were obtained at 4.7 T. (B) The average MRI signal intensity of mouse liver 6 min after injection of either GdL_1 or Gadavist™ in control mice (black bars) *versus* mice pretreated with ATN-224 (white bars). The columns on the right show average liver signal intensities at 13 min after injection with Multihance™. The data were compared using a two-tailed student t-test. *$p < 0.05$ (n=3); error bars reflect ± SD. (C) Total Cu and Gd (μg/g tissue) in various tissues collected from control mice (black bars) and from mice pretreated with ATN-224 (white bars) 6 min after the injection of GdL_1. Tissue copper levels relative to tissue wet weight were determined by ICP-MS. The data were compared using a two-tailed student t-test. *$p < 0.05$ (n=3); error bars reflect ± SD.

Mice were also imaged using two different Gd-based agents as controls, Gadavist (an extracellular agent) and Multihance (a hepatobiliary agent). After injection of an equivalent amount of Gadavist, the signal intensity of liver gained intensity as expected for a typical extracellular agent but only by ~8%. Like GdL_1, the signal gain in liver reached a maximum at ~6 min then returned to pre-injection baseline values at about the same clearance rate as GdL_1. In mice pretreated with ATN-224, the liver enhancement was unchanged, consistent with a lack of affinity of Gadavist for Cu^{2+}. Given that the possibility a small amount of GdL_1 may clear via hepatobiliary excretion (a complete biodistribution study has not been done), it was important to perform a similar set of control experiments using a known hepatobiliary agent, Multihance, to determine whether ATN-224 treatment might alter liver function. Those imaging results are also presented in Figure 6B. Since the clearance of Multihance in liver was significantly slower than either GdL_1 or Gadavist, the signal intensity data shown here reflect the maximum values at 13 min rather than at 6 min. As shown, liver image enhancement resulting from the passage of Multihance through the liver was identical in untreated mice versus mice pretreated with ATN-224, showing that liver function is unaltered by ATN-224. Therefore, the decreased intensity we observed when using GdL_1 must reflect a decrease in freely available Cu^{2+} in liver.

3. CONCLUSIONS

In this study, we investigated whether a new macrocyclic gadolinium complex, GdL_1, could act as a Cu^{2+}-responsive MRI contrast agent. We also examined the physical-chemical properties of the ternary GdL_1-Cu^{2+}-HSA complex that resulted

in a magnified longitudinal r_1 relaxivity (20 MHz) of 22.6 $mM^{-1}s^{-1}$. Our results showed that the observed r_1 enhancement due to the slow tumbling of the ternary complex was sufficient to allow detection of μM levels of freely available Cu^{2+} in the liver by T_1-weighted MR imaging, even at 4.7T. After injection of GdL_1 into healthy untreated mice, the liver was nicely enhanced at 6 min, and image contrast returned to background levels after ~ 20 min. However, when mice were treated with ATN-224, the MR signal gain in liver images was ~50% less compared to control animals. The lower contrast enhancement observed in the liver of mice pretreated with ATN-224 paralleled the reduction in total liver copper as detected by ICP-MS. Based on the ICP results, one can estimate the concentration of GdL_1 in liver at 6 min and ask the question of whether the decreased levels of Cu as detected by ICP-MS are consistent with the imaging results. The total amount of Gd in liver at 6 min was 40 μg/g wet tissue. If one assumes that GdL_1 remains largely extracellular and that the extracellular fraction of wet liver is ~24-26%,[71,72] then the GdL1 concentration can be estimated as ~1 mM (40 μg/g divided by 157 g/mol = 0.25 μmol/g = 0.25 μmol/0.26 mL = 1 mM). This same calculation for Cu gives a total [Cu] of 0.36 mM in liver of control mice (6 μg/g) and 0.18 mM in livers after treatment with ATN-224 (3 μg/g). Although not all of the Cu^{2+} is extracellular, a 50% change in available Cu would easily be detected using GdL_1 even if r_1 is no higher than 9 $mM^{-1}s^{-1}$ at 4.7T. One would expect to see even more dramatic changes in MRI signal intensity in liver if these experiments had been performed at typical clinical imaging fields, 1.5T or 3T.

The second goal of this study was to identify the Cu^{2+} donor atoms on GdL_1, the donor atoms in the ternary GdL_1-Cu^{2+}-HSA complex, and the location of the GdL_1-Cu^{2+} binding site in HSA. The fact that Cu^{2+} has only one high-affinity site in HSA, the N-terminal site,[55,57] it is reasonable to assume that GdL_1 also binds at this site by contributing donor atoms to Cu^{2+}. This model is consistent with the changes in the Cu^{2+} coordination sphere as reported by EPR and X-ray absorption spectroscopy (XAS) data. The combined results indicate that the Cu^{2+} binds to GdL_1 via a single tertiary N atom and two carboxylate O atoms on GdL_1 and a single water molecule to form a distorted tetragonal complex. The Cu^{2+} center in GdL_1-Cu^{2+}-HSA ternary complex is most consistent with coordination by four equatorial nitrogen donor atoms from the protein and one or two axial O/N donor from GdL_1 resulting in distorted octahedral/square pyramidal geometry. The slight coordination changes in the Cu^{2+} center with GdL_1 in the presence of HSA results in a stable ternary complex that results in a surprisingly high r_1 relaxivity at 20 MHz.

In summary, our study shows that GdL_1 can be used as a sensor of excess freely available Cu^{2+} ions in tissue. In the presence of HSA, the freely available Cu^{2+} forms a stable ternary complex GdL_1-Cu^{2+}-HSA that magnifies the r_1 relaxivity to such an extent that *in vivo* detection of exchangeable Cu^{2+} MR imaging was possible. To our knowledge, this is the first time that extracellular copper levels in the liver could be detected and with a remarkable statistical difference. Although this work has not included a mouse disease model to validate the results obtained here, there is enough evidence to suggest that this sensor can be used in mouse models with known abnormal levels of copper. The total serum copper levels can be markedly elevated in acute liver failure due to its release of excess copper ions from liver tissue stores. This results in elevated total serum Cu^{2+} not bound to ceruloplasmin referred to as "free-copper".[73] For example, Wilsons' disease patients reported the significantly higher concentrations of serum non-ceruloplasmin copper (>4.0μM) in the blood[74] and hepatic copper content of >250μg per gram of dry liver weight.[75,76] Similarly, deficiency of copper has been reported in a variety of genetic, neurological, cardiovascular and metabolic diseases.[9,77] Furthermore, it has recently been shown that elevated serum and tumor copper levels are linked to the progression of cancer malignancy[78] and also plays an important role in the regulation of sleep-related and arousal behaviors.[79] Therefore, we believe that the observations reported here using GdL_1 will catalyze discoveries of Cu^{2+}-responsive MRI agents for imaging acute liver conditions such as that found in Wilsons diseases or elevated copper levels in other disease conditions.

ASSOCIATED CONTENT

Supporting Information.

The SI contains the synthesis details for preparing the Gd complexes, the experimental details of the relaxometric experiments, titrations, ^{17}O NMR experiments, EPR spectra, EXAFS spectra, cyclic voltammetry, computational model details, and MR images.

AUTHOR INFORMATION

Corresponding Author
* E-mail: dean.sherry@utsouthwestern.edu; sherry@utdallas.edu.

Author Contributions
All authors read and approved the manuscript.

ACKNOWLEDGMENTS

Financial support from the National Institutes of Health (DK-095416 and EB-015908), the American Diabetes Association (ADA 7-12-IN-42) and the Robert A. Welch Foundation (AT-584) is gratefully acknowledged. We thank the staff at Beamline 9-3, Stanford Synchrotron Radiation Light source (SSRL) for support in XAS data collection. We also thank Dr. Alexendar Funk for help with the mouse imaging experiments at UTSW, Drs. Hien Q. Nguyen and Alexios Papadimitrators for their support and training in the ICP-MS, EPR experiments at UT Dallas, and Dr. Limei Zhang at University of Nebraska-Lincoln for discussions on XAS data collection and analysis.

ABBREVIATIONS

HSA, Human Serum Albumin, XAS, X-ray absorption spectroscopy, MRI, Magnetic resonance imaging.

REFERENCES

1. Puig, S.; Thiele, D.J. Molecular mechanisms of copper uptake and distribution. *Curr. Opin. Chem. Biol.* **2002**, 6, 171-180.
2. Maryon, E.B.; Molloy, S.A.; Zimnicka, A.m.; Kaplan, J.H. Copper entry into human cells: progress and unanswered questions. *Biometals*. **2007**, 20, 355- 364.
3. Linder MC, Wooten L, Cerveza P, Cotton S, Shulze S, Lomeli N. Copper Transport. *Am J Clin Nutr.* **1998**,67,965S–971S.
4. Prohaska, J.R.; Gybina, A.A. Intracellular coppert transport in mammals. *J. Nutr.* **2004**, 134, 1003-1006.
5. Lutsenko, S.; Barnes, N.L.; Bartee, M.Y.; Dmitriev. O.Y. Function and Regulation of Human Copper-Transporting ATPases. *Physiol Rev.***2007**. 87,1011-1046.

6. Balamurugan K.; Schaffner W. Copper homeostasis in eukaryotes: teetering on a tightrope. *Biochim Biophys Acta*. **2006**,1763,737–746.
7. Macreadie I.G. Copper transport and Alzheimer's disease. *Eur. Biophys. J*. **2008**, 37, 295–300.
8. Waggoner, D.J.; Bartnikas, T.B.; Gitlin, J.D. The role of copper in neurodegenerative disease. *Neurobiol. Dis.* **1999**, 6, 221-230.
9. Que, E.L.; Domaille, D.W.; Chang, C.J. Metals in neurobiology: probing their chemistry and biology with molecular imaging. *Chem. Rev.* **2008**, 108, 1517–1549.
10. Zatta, P.; Frank A. Copper deficiency and neurological disorders in man and animals. *Brain Res Rev*. **2007**, 54,19–33.
11. Bush, A.I. Metals and neuroscience**.** *Curr. Opin. Chem. Biol*. **2000**, 4, 184-191.
12. Brown, D.R.; Qin, K.; Herms, J.W.; Madulaung, A.;Manson, J.; Strome, R.; Fraser, P.E.; Kuck, T.; von Bohlen A.; Schulz- Schaeffer, W.; Giese, A.; Westway, D.; Kretzscmar, H. The cellular prion protein binds copper in vivo. *Nature*, **1997**, 390, 684-687.
13. Morgan, M. T.; Bagchi, P.; Fahrni, C. J. Fluorescent probes for monovalent copper. *Encyclopedia of Inorganic and Bioinorganic Chemistry*.**2013**, 1–19.
14. Rae, T.D.; Schmidt, P.J.; Pufahl,R.A.; Culotta,V.C.; O'Halloran, T.V. Undetectable intracellular free copper: the requirement of a copper chaperone for superoxide dismutase. *Science*, **1999**, 284, 805.
15. Gaggelli, E.; Kozlowski, H.; Valensin, D.; Valensin, G. Copper homeostasis and neurodegenerative disorders (Alzheimer's, prion, and Parkinson's diseases and amyotrophic lateral sclerosis). *Chem. Rev.* **2006**, 106, 1995-1998.
16. Waggoner, D.J.; Bartnikas, T.B.; Gitlin, J.D. The role of copper in neurodegenerative disease. *Neurobiol. Dis.* **1999**, 6, 221-230.
17. Desai, V.; Kaler, S.G. Role of copper in human neurological disorders. *Am J Clin Nutr***. 2008,** 88, 855S-858S.
18. Multhaup, G.; Schlicksupp, A.; Hesse, L.; Beher, D.; Ruppert, T.; Masters, C.L.; Beyreuther, K. The amyloid precursor protein of Alzheimer's disease in the reduction of copper(II) to copper(I). *Science*, **1996**, 271, 1406-1409.
19. Bertini, I.; Rosato, A. Menkes disease. *Cell Mol. Life Sci.* **2008**, 65, 89-91.
20. Kaler, S.G. ATP7A-related copper transport diseases-emerging concepts and future trends. *Nat. Rev. Neurol.* **2011**, 7, 15-29.
21. Lutsenko, S.; Gupta, A.; Burkhead, J.L.; Zuzel, V. Cellular multitasking: the dual role of human Cu-ATPases in cofactor delivery and intracellular copper balance. *Arch. Biochem. Biophys.* **2008**, 476, 22-32.
22. Cox, D.; Moore, S.D. Copper transporting P-type ATPases and human disease. *J Bioenerg. Biomembr.* **2002**, 34, 333-338.
23. Valentine, J.S.; Doucette, P.A.; Potter, S.Z. Copper-zinc superoxide dismutase and amyotrophic lateral sclerosis. *Annu. Rev. Biochem*. **2005**, 74, 563- 572.
24. Peng, F.; Lutsenko, S.; Sun, X.; Musik, O. Positron emission tomography of copper metabolism in the Atp7b-/- knock-out mouse model of Wilson's disease. Mol. Imaging Biol. 2012, 14, 70-78.
25. Peng, F. Positron emission tomography for measurement of copper fluxes in live organisms. *Ann. N.Y. Acad. Sci.* **2014**,1314, 24–31.
26. Aime, S.; Botta, M.; Terreno, E. Gd (III)-based contrast agents for MRI. *Adv. Inorg. Chem*., **2005**, 57,173-232.
27. Aime, S.; Botta, M.; Fasano, M.; Terreno, E. Lanthanide (III) chelates for NMR biomedical applications. *Chem. Soc. Rev*.,**1998**, 27, 19-29.
28. Caravan, P.; Ellison, J. J.; McMurry, T.J; Lauffer, R.B. Gadolinium(III) Chelates as MRI Contrast Agents: Structure, Dynamics, and Applications. *Chem. Rev*., **1999**, 99, 2293-2352.
29. Moats, R.A.; Fraser, S.E.; Meade, T.J. A 'smart' magnetic resonance imaging agent that reports on specific enzymatic activity. *Angew. Chem. Int. End. Eng.*, **1997**, 36, 726-732.
30. Raghunand, N.; Howison, C.; Sherry, A.D.; Zhang, S.; Gillies, R.J. Renal and Systemic pH Imaging by Contrast-Enhanced MRI. *Magn. Reson. Med.* **2003**, 49, 249-257.
31. Aime, S.; Botta, M.; Gianolia, E.; Terreno, E. A p(O(2))-Responsive MRI Contrast Agent Based on the Redox Switch of Manganese(II / III) - Porphyrin Complexes. *Angew. Chem. Int. Ed.* **2000**, 39, 747-754.
32. Berkowitz, B.A.; Wilson, C.A.; Hatchell, D.L.; London, R.E. Quantitative-Determination of the Partial Oxygen-Pressure in the Vitrectomized Rabbit Eye In vivo Using F-19 NMR. *Magn Reson Med.* **1991**, 21, 233–241.
33. Que, E.L.; Chang, C.J. A smart magnetic resonance contrast agent for selective copper sensing. *J. Am. Chem. Soc.* **2006**, 128, 15942.
34. Que, E. L.; Gianolio, E.; Baker, S. L.; Wong, A. P.; Aime, S.; Chang, C. J. Copper-responsive magnetic resonance imaging contrast agents. *J. Am. Chem. Soc.* **2009**, 131, 8527.
35. Li, W.S.; Luo, J.; Chen, Z.N. A gadolinium(III) complex with 8-amidequinoline based ligand as copper(II) ion responsive contrast agent. *Dalton Trans.* **2011**, 40, 484-492.
36. Jang, J.H.; Bhuniya, S.; Kang, J.; Yeom, A.; Hong, K.S.; Tim, J.S., Cu^{2+}-Responsive Bimodal (Optical/MRI) contrast agent for cellular imaging, *Organic Letters*, **2013**,15, 4702-4705.
37. Zhang, X.; Jing, X.; Liu, T.; Han, G.; Li, H.; Dun, C.; Dual-functional Gadolinium Based Copper (II) probe for selective magnetic resonance Imaging and florescence sensing, *Inor. Chem*. **2012**, 51, 2325-2331.
38. Hirayama, T.; Van de Bittner, G.C.; Gray, L.W.; Lutsenko, S.; Chang, C.J. Near-infrared fluorescent sensor for in vivo copper imaging in a murine Wilson disease model. *PNAS*, **2012,** 190, 2228-2233.
39. Jordan, M.V.C.; Lo, S.; Chen, S.; Preihs, C.; Chirayil, S.; Zhang, S.; Kapur, P.; Li, W.; Leon-Rodriguez, L.M.D.; Lubag, A.J.M.; Rofsky, N.M.; Sherry, A.D. Zinc-sensitive MRI contrast agent detects differential release of Zn(II) ions from the healthy vs. malignant mouse prostate. *PNAS*, **2016**, 113, E 5464-E5471.
40. Lubag, A.J.M.; Leon-Rodriguez, L.M.D.; Burgess, S.C.; Sherry, A.D. Noninvasive MRI of β-cell function using a Zn2+-responsive contrast agent. *PNAS*, **2011**, 108, 18400-18405.
41. Yu, J.; Martins, A.F.; Preihs, C.; Clavijo-Jordan,V.; Chirayil, S.; Zhao, P.; Wu, Y.; Nasr, K.; Kiefer, G.E.; Sherry, A.D. Amplifying the sensitivity of Zinc(II) responsive MRI contrast agents by altering water exchange rates. *J. Am. Chem. Soc.*, **2015**, 137, 14173–14179.
42. Esqueda, A. C.; López, J. A.; Andreu-de-Riquer, G.; Alvarado-Monzón, J. C.; Ratnakar, J.;Lubag, A. J. M.; Sherry, A. D.; De León-Rodríguez, L. M. A new gadolinium-based MRI zinc sensor. *J. Am. Chem. Soc.* **2009**, 131,11387- 11391.
43. Gaur, A.; Klysubun, W.; Nair, N.N.; Shrivastava, B.D.; Prasad. J.; Srivatava, K. XAFS study of copper(II) complexes with square planar and square pyramidal coordination geometries**.** *Journal of Molecular Structure*, **2016**,1118, 212-218.
44. Laussac, J.P; Sarkar, B. Characterization of the copper(II)- and nickel(II)-transport site of human serum albumin. Studies of copper(II) and nickel(II) binding to peptide 1-24 of human serum albumin by 13C and 1H NMR spectroscopy. *Biochemistry*, **1984**, 23,2832-2838
45. Zgirski, A.; Frieden, E. Binding of Cu(II) to non-prosthetic sites in ceruloplasmin and bovine serum albumin. *J. Inorg. Biochem*. **1990**, 39, 137-148.

46. Bal, W. Christodoulou, J.; Sadler, P.J.; Tucar, A. Multi-metal binding site of serum albumin. *J. Inorg. Biochem.* **1998**, 70, 33-39.
47. Lu, J.; Stewart, A.J.; Sadler, P.J.; Pinheiro, T.J.T.; Blindauer, C.A. Albumin as a zinc carrier: properties of its high-affinity zinc-binding site. *Biochem. Soc. Trans*. **2008**, 36, 1317-1321.
48. Shakdofa, M.; Shtaiwi, M.; Morsy, N.; Abdel-raseel, T.M.A. Metal complexes of hydrazones and their biological, analytical and catalytic applications: A review. *Main Group Chemistry,* **2014**, 13, 187-218.
49. Zhang, G.; Zhong, W.; Wei, Z.; Liu, Z.; Liu, X. Roles of phenol groups and auxiliary ligand of copper(ii) complexes with tetradentate ligands in the aerobic oxidation of benzyl alcohol. *Dalton Transactions*, **2017**, 46, 8286-8297.
50. Vymazal, J.; Bulte, J. W. M.; Frank, J. A.; Chiro, G. D.; Brooks, R. A. Frequency dependence of MR relaxation times I. Paramagnetic ions. *J. Magn. Reson. Imaging*, **1993**, 3, 637–640.
51. Casella, L.; Gullotti, M.; Pallanza, G.; Pinter, A.; Marchesini, A. Spectroscopic and binding studies of azide to type-2-copper-depleted ascorbate oxidase from zucchini. *Biol. Metals*., **1991**, 4, 81-87.
52. Job, P. Formation and Stability of Inorganic Complexes in Solution. Ann.Chim(Paris), **1928**, 113-115.
53. Guo, M.; Zou, J.; Li, P.; Shang, Z.; Hu, G.; Yu, Q.; Binding interaction of gatifloxacin with bovine serum albumin. *Anal. Sci.* **2004**, 20, 465-470.
54. Cabaniss, S.E.; Shuman, M.S. Combined ion selective electrode and fluorescence quenching detection for copper-dissolved organic matter titrations. *Anal. Chem.* **1986**, 58, 398-401.
55. Hureau, C.; Eury, H.; Guillot, R.; Bijani, C.; Sagen, S.; Solari, P.; Guillon, E.; Faller, P.; Dorlet, P. X-ray and Solution Structures of Cu^{II}GHK and Cu^{II}DAHK Complexes: Influence on Their Redox Properties. *Chem. Eur. J.* **2011**, 17, 10151-10160.
56. Bal, W.; Christodoulou, J.; Sadler, P.J.; Tucker, A. Multi-metal binding site of serum albumin. *Journal of Inorganic Biochemistry,* **1998**, 70, 33-39.
57. Rozga, M.; Sokolowska, M.; Protas, A.M.; Bal, W., Human serum albumin coordinates Cu(II) at its N-terminating binding site with 1pM affinity. *J. Biol. Inorg .Chem*. **2007**,12,913-918.
58. Bal, W.; Sokołowska, M.; Kurowska, E.; Faller, P. Binding of transition metal ions to albumin: Sites, affinities and rates. *Biochim. Biophys. Acta*, **2013**, 1830, 5444-5455.
59. Neumann, P.Z.; Sass- Kortsark, A. The state of copper in human serum: evidence for an amino acid-bound fraction. *Journal of Clinical Investigation*, **1967**, 46, 646-658.
60. Tweedle, M. F.; Hagan, J. J.; Kumar, K.; Mantha, S.; Chang, C. A. Reaction of gadolinium chelates with endogenously available ions. *Magn. Reson. Imaging* **1991**, 9, 409–415
61. Xio, Y.; Zhao, G.; Fang, X.; Zhao, Y.; Wang, G.; Yang, W.;Xu, J. A smart copper(II)-responsive binuclear gadolinium(III) complex-based magnetic resonance imaging contrast agent. *RSC Adv*, **2014**, 4, 34421- 34427.
62. Sadler, P.J.; Viles, J.H., 1H and (113)Cd NMR Investigations of Cd(2+) and Zn(2+) Binding Sites on Serum Albumin: Competition with Ca(2+), Ni(2+), Cu(2+), and Zn(2+).*Inorg. Chem*. **1996**, 35, 4490-4496.
63. Martins, D.A.; gourea, L.R.; Muniz, G.S.; Louro, S.; Gama, D.; Soeiro, M.; Teixeira, L.R., Norfloxacin and N-Donor Mixed-Ligand Copper(II) Complexes: Synthesis, Albumin Interaction, and Anti- Trypanosoma cruzi Activity.*Bioinorganic chemistry and application*, **2016,** 1-11.
64. Sano, M.; Komorita, S.; Yamatera, H. XANES spectra of copper(II) complexes: correlation of the intensity of the 1s .fwdarw. 3d transition and the shape of the complex. *Inorg. Chem* **1992**, 31, 459-463.
65. Askwith, C.; Eide, D.; Van Ho, A.; Bernard, P.S.; Li L.; Davis-Kaplan, S.; Sipe, D.M.; Kaplan J. The FET3 gene of S. cerevisiae encodes a multicopper oxidase required for ferrous iron uptake. *Cell*, **1994**, 76,403–10.
66. Linder, M.C.; Massaro, E.J., editor. *Handbook of copper pharmacology and toxicology.* Humana Press: New Jersey; **2002**. 3–32.
67. Vural, H.; Uzun, K.; Uz, E.; Kocgigil, A.; Cigli, A.; Akyol, O. Concentration of copper, zinc and various elements in serum of patients with bronchial asthma. *J,Trace Elements Med.Bio*l., **2000**, 14, 88-91.
68. Alebic-Juretic. A.; Frkovic, A. Plasma copper concentrations in pathological pregnancies. *J. of Trace Elements in Medicine and Biology*, **2005**, 19,191-194.
69. Linder, M.C.; Wooten, L.; Cerveza, P.; Cotton, S.; Shulze, S.; Lomeli, N. Copper transport. *Am J Clin Nutr.*, **1998**, 67,965S–971S.
70. Lowndes, S.A.; Sheldon, H.V.; Cai, S.; Taylor, J.M.; Harris, A.L. Copper chelator ATN-224 inhibits endothelial function by multiple mechanisms. *Microvascular Research*, **2009**, 77, 314-326.
71. Barratt, T.M.; Walser, M. Extracellular fluid in individual tissues and in whole animals: the distribution of radiosulfate and radiobromide. *J.Clin.Invest*. **1969**,48,56-66.
72. Guo, S.L.; Su, L.N.; Zhai, Y.N.; Chirume, W.M.; Lei, J.Q.; Zhang, H.; Yang, L.; Shen, X.P.; Wen, X.X.; Guo, Y.M. The clinical value of hepatic extracellular volume fraction using routine multi phasic contrast-enhanced liver Ct for staging liver fibrosis. *Clin. Radiol*. **2017**, 72, 242-246.
73. Ferenci, P.; Czlonkowska, A.; Merle, U.; Ferenc, S.; Gromadzka, G.; Yurdaydin, C.; Vogel, W.; Bruha, R.; Schmidt, H.T.; Strmmel, W. Late-onset Wilson's disease. *Roenterology*, **2007**, 132, 1294-1298.
74. Frommer, D.J. Direct measurement of serum non-caeruloplasmin copper in liver disease. *Clinica Chimica Acta*, **1976,** 68, 3030-307.
75. Yang, X.; Tang X.P.; Zhang, Y.H.; Luo, K.Z.; Jiang Y.F.; Luo H.Y.; Lei J.H.; Wang, W.L.; Li, M.M.; Chen, H.C.; Deng, S.L.; Lai, L.Y.; Liang, J., Zhang, M.; Tian, Y.; Xu, Y. Prospective evaluation of the diagnostic accuracy of hepatic copper content, as determined using the entire core of a liver biopsy sample. *Hepatology.* **2015,** 62, 1731-41.
76. Poujois, A; Trocello, J-M; Djebrani-Oussedik, N; Poupon, J; Collet, C; Girardot-Tinant, N; Sobesky, R; Habès, D; Debray, D; Vanlemmens, C; Fluchère, F; Ory-Magne, F; Labreuche, J; Preda, C; Woimant, F. Exchangeable copper: a reflection of the neurological severity in Wilson's disease. *European Journal of Neurology*. **2017**, 24,154-160.
77. Heffern, M. C.; Park, H. M.; Au-Yeung, H. Y.; Van de Bittner, G. C.; Ackerman, C. M.; Stahl, A. Chang, C. J. In vivo bioluminescence imaging reveals copper deficiency in a murine model of nonalcoholic fatty liver disease. *Proc. Natl. Acad. Sci. USA* **2016**, *113*, 14219-14224.
78. Mumper, R.J.; Gupte, A. Elevated copper and oxidative stress in cancer cells as a target for cancer treatment. *Cancer treatment Reviews*, **2009**,35,32-46.
79. Xiao, T; Ackerman, C.M.; Carroll, E.C.; Jia, S.; Hogland, A.; Chan, J.; Thai, B.; Liu, C.S.; Iscacoff, E.Y.; Chang, C.J. Copper regulates rest-activity cycles through the locus coeruleus-norepinephrine system. *Nat. Chem. Biol.* **2018,** 14,655–663.
80.

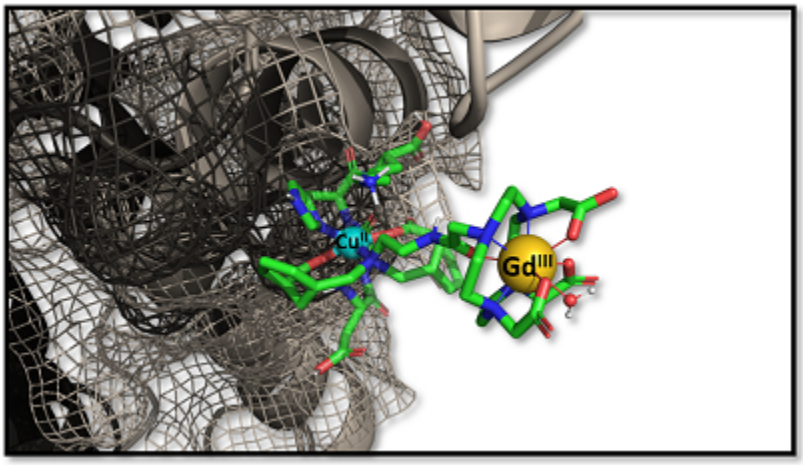

106x61mm (96 x 96 DPI)